Radio Observations of Solar Eruptions

N. Gopalswamy
NASA Goddard Space Flight Center, Greenbelt, MD USA
gopals@fugee.gsfc.nasa.gov

Abstract

Coronal mass ejections (CMEs) are composed of multithermal plasmas, which make them produce different radio signatures at different wavelengths. The prominence core of CMEs are of the lowest temperature and hence optically thick at microwave frequencies and hence are readily observed. The Nobeyama Radioheliograph has exploited this fact and observed a large number of prominence eruptions over most of solar cycle 23 and parts of cycle 22. This paper reviews recent studies on prominence eruptions and their contributions for understanding the CME phenomenon. In particular, the following issues are discussed: (i) the statistical and physical relationship between CMEs and the radio prominence eruptions, and how this relationship manifests as a function of the solar cycle; (ii) The asymmetry of prominence eruptions between northern and southern hemispheres; (iii) the relationship between prominence eruptions and CME cores; (iv) the implications of the cessation of high-latitude PEs before the reversal of the global solar magnetic field, and (v) the implications of the high-latitude PEs and CMEs for the modulation of galactic cosmic rays. Finally, the importance of the Nobeyama Radioheliograph data to future missions such as STEREO and Solar-B are discussed.

Key words: Sun: activity — Sun: flares — Sun: corona — Sun : radio

1. Introduction: Sun in Microwaves

A microwave imager such as the Nobeyama Radioheliograph (NoRH, Nakajima et al., 1994) observes a large number of features on the Sun occurring at various layers of the solar atmosphere: (1) the quiet solar disk at 10,000 K, which is the upper chromospheric layer of the Sun, optically thick in microwaves. (2) Active regions, which appear as small bright patches due to free-free emission from the active region loops and gyroresonance emission from sunspots. The sunspots appear as the strongest features in active regions when there is no flaring. (3) Filaments are cool (∼8000 K) features suspended in the hot corona against a brighter (Tb ∼10,000 K) solar disk and hence appear as dark linear features, somewhat similar to what is seen in Hα. (4) Prominences are the same as filaments observed above the solar limb, but appear bright because the background now is not the solar disk, but the cold sky. The corona itself is optically very thin in microwaves and contributes only a few 100 K to the observed brightness temperature. (5) Sometimes mounds consisting of AR loops (Tb >10,000 K) are seen at the limb. (6) Bright post-eruption loops are observed when active regions erupt. When quiescent filaments erupt, the post-eruption loops take the form of an arcade. The brightness temperature of the post-eruption structures depends on the emission mechanism. Gyrosynchrotron emission from flare loops can exceed 1 MK. (7) On rare occasions, one can also observe dimming (deficit of free-free emission) above the limb (Gopalswamy, 2003). Many of these features can be seen in the 17 GHz microwave image obtained on 2000 February 26 at 23:51:24 UT (see Fig.1). Various features discussed above are marked. This snapshot illustrates the wealth of information the microwave images provide on the Sun. Time series of such images capture the dynamic Sun and provide quantitative measurement of many physical parameters corresponding to the chromosphere and corona of the Sun. The prominence seen above the northeast limb in Figure 1 is eruptive as part of a coronal mass ejection (CME) also shown superposed. Hundreds of such eruptions have been documented on the NoRH web site (http://solar.nro.nao.ac.jp/norh/html/prominence/). Filament eruptions are similar to the "disparition brusques" observed in Hα. Both case studies (e.g., Hanaoka et al., 1994; Gopalswamy et al., 1996; 1999; Hanaoka and Shinkawa, 1999; Uralov et al., 2002; Kundu et al. 2004) and statistical investigations (Gopalswamy et al., 2003a; Hori, 2000; 2002) have been performed on these eruptions. This paper provides a summary of the important results on solar eruptions, especially in conjunction with data from the Solar and Heliospheric Observatory (SOHO) mission.

2. Case Studies of Solar Eruptions

2.1. Studies in the pre-SOHO Era

When routine NoRH observations of the Sun commenced in 1992, there was no spaceborne coronagraph available for comparing microwave eruptions with white light CMEs. Fortunately, the soft X-ray telescope (SXT) on board the Yohkoh satellite was observing solar eruptions, so most of the early studies involved coronal changes in X-rays in association with prominence eruptions (PEs). The X-ray and microwave signatures have been reviewed before (Gopalswamy, 1999; Cliver and Hudson, 2002).

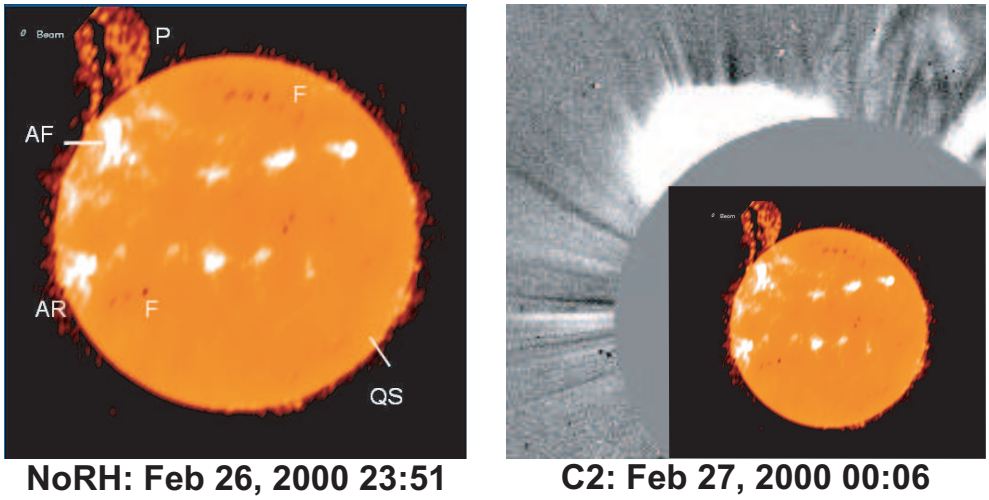

Fig. 1. *Left*: A NoRH image at 17 GHz obtained on 2000 February 26 at 23:51 UT with various observed features marked: QS - quiet Sun at 10,000 K, F - filament, AR - active region, AF - post-eruption arcade formation, and P - prominence. The beam size of NoRH is shown at the top left. *Right*: The image on the left superposed on a white light coronal image taken by SOHO's Large Angle and Spectrometric Coronagraph (LASCO) at 00:26 UT on 2000 February 27. Note the good position angle correspondence between the CME and the eruptive prominence.

The use of NoRH for the study of eruptive events started with the observation of a spectacular PE observed during 1992 July 30-31 (Hanaoka et al., 1994). This event displayed all the signatures of a major eruption: eruptive prominence followed by post-eruption arcade extending along the neutral line, and two-ribbon structure in Hα (see Fig.2). The prominence ascended with a speed of $\sim$100 km/s, and had an appearance very similar to what was observed in Hα, especially when the Hα images were degraded to the resolution of the microwave images. Unfortunately, there was no white light coronagraphic observation at that time, so the full picture of the eruption including the CME could not be obtained. However, a linear soft X-ray feature was observed moving away from the neutral line before the arcade formation (see Fig.2), which is likely to be part of the associated CME owing to its higher speed (160 km/s) and motion ahead of the prominence. The post-eruption arcade, normally observed in X-rays and EUV, was also detected in microwaves owing to the enhanced free-free emission from the hot dense loops making the arcade. The soft X-ray arcade had a temperature of $\sim$3.6 MK and a density of $\sim 2.4 \times 10^9$ cm^{-3}. This hot dense plasma produced a 17 GHz brightness temperature of $\sim$7500 K above the quiet Sun level ($\sim$10,000 K) via free-free emission. This event also demonstrated that it is possible to obtain quantitative information on various features in the eruption region. For example, the observed brightness temperature and the dimensions of the arcade can be used to infer the kinetic temperature of the post-eruption structure. The combined X-ray and microwave observations were found to be consistent with the Carmichael-Sturrock-Hirayama-Kopp-Pneuman (CSHKP) model (Svestka and Cliver, 1992) of prominence eruptions. A version of the model from Anzer and Pneuman (1982) is shown in Fig.2. The nested helices marked "prominence" may be taken to represent the cavity identified in CMEs as flux ropes.

Another very slow microwave prominence eruption (see Fig.3) was observed during 1993 July 10-11, which had an average speed of only 3.7 km/s over a period of $\sim$6 hours (Gopalswamy et al., 1996). Fortunately, the Yohkoh observations were extensive in this case and the frontal structure of the CME, which moved with a speed of 15 km/s, was observed in soft X-rays. A post-eruption arcade (AF) was also observed in Hα and microwaves (see Fig.3). The mass of the X-ray frontal structure was estimated to be $\sim 2.6 \times 10^{14}$ g, only slightly lower than the average mass of SOHO CMEs (Vourlidas et al., 2002). It must be pointed out that SOHO has observed many CMEs with mass of only $\sim 10^{13}$ g. The event also showed post eruption structure in X-rays, Hα and microwaves (Gopalswamy et al. 1997). Some of the important conclusions of this study were that a coronal volume much larger than that of the prominence was involved in the eruption and that the pre-eruption position of the leading edge was $\sim$0.3 R$_\odot$ above the solar surface. Another event with the opening of an X-ray structure 5 times as large as the microwave eruptive prominence was reported (Gopalswamy et al., 1998a). Thus the microwave observations have started contributing to the study of the early phase of CMEs, typically not observed by coronagraphs due to the occulting disk they employ.

Gopalswamy and Hanaoka (1998) tracked a long ($\sim$475,000 km) north-south filament during its disk passage for 2 weeks until it erupted above the west limb at a height of 175,000 km. At the start of the eruption, the prominence was massive ($\sim 6 \times 10^{16}$ g). The eruption was slow and the height-time measurements of the prominence could be fit to a second order polynomial (constant acceleration, $\sim$11 m/s^2). The final speed was only $\sim$70 km/s

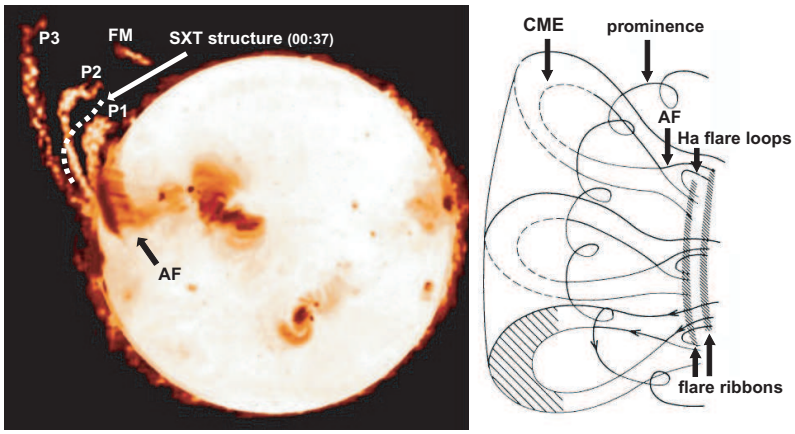

Fig. 2. The prominence eruption event of 1992 July 30-32 studied by Hanaoka et al. (1994). *Left*: Three stages of the prominence (P1 at ∼ 00:35, P2 at ∼00:45, and P3 at ∼01:25 UT) superposed on a Yohkoh SXT image showing the post eruption arcade (AF) under the eruptive prominence. A fragment of the falling prominence material (FM) is identified. The SXT structure at 00:37 is also shown, which was ahead of the prominence. *Right*: A version of the CSHKP model from Anzer and Pneuman (1982) that fits the observation. The helical structure may actually be more than just the eruptive prominence. It may represent the CME cavity. The Hα flare ribbons form the footpoints of the SXT post-eruption arcade (AF). Hα flare loops are the cooled form of the SXT loops in AF. There was no white light observation to provide information on the overlying CME.

when the prominence reached the edge of the NoRH field of view. There was no simultaneous white light observation, but the difference between white light images taken on consecutive days clearly indicated a major change in the streamer, confirming an associated coronal eruption. An extensive coronal dimming was observed in association with the prominence eruption (see Fig.4) with a long post-eruptive arcade formed close to the limb. From the dimming, the mass of the depleted coronal material was estimated to be $\sim 2 \times 10^{15}$ g, which is the typical mass of large CMEs. This is smaller than the initial prominence mass, but there was large down flow of material as the prominence rose. Thus even if only a small fraction of the prominence material escaped, it must have carried a mass comparable to the hot material ejected from the corona. Based on the extent of the dimming region and the north-south orientation of the pre-eruption filament, Gopalswamy and Hanaoka (1998) suggested that the cavity of the CME is not expected to be seen above the northwest limb in such a configuration and that an east-west filament would show the cavity. This was confirmed in a recent study involving a large number of CMEs (Cremades and Bothmer, 2004).

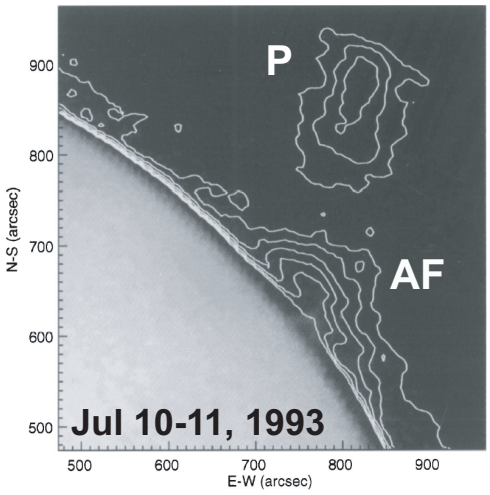

Fig. 3. Microwave eruptive prominence (P) and the post-eruption arcade (AF) presented as contours overlaid on an Hα picture. The Hα loop prominence (post-flare loops) can be seen faintly above the limb, partly coinciding with the AF contours (adapted from Gopalswamy et al. 1997).

Eruptions occurring close to the limb are easy to observe because of the weak coronal background at many wavelengths. This is usually not the case for disk eruptions. Hanaoka and Shinkawa (1999) studied two NoRH erupting filaments (1992 November 5 and 1994 February 20) at 17 GHz. Shortly after the apparent disappearance, a transient reduction occurred in the brightness of the nearby plage regions. The disappearance of the filament is due to the heating of the filaments at least to the temperature of the microwave disk, but to a temperature below that of the plage region. This is because the plages returned to their original brightness after the passage of the heated filament. It was also found that after the initial increase, the brightness temperature of the filaments was rather constant during their motion. Once heated, the filament disappears in Hα because of the spectroscopic nature of the observation. The microwave emission is via thermal free-free emission, which is a continuum emission, so the filament does not disappear. The lower limit of the energy supplied to the filament in the heating process was estimated to be $\sim 3.6 \times 10^{26}$ erg, a few orders of magnitude smaller than the kinetic energy of the filament or the energy of the associated flare. In some cases, the filament shows expansion but the average brightness temperature decreases due the increased area of the filament, but still remains optically thick (Gopalswamy, 1999).

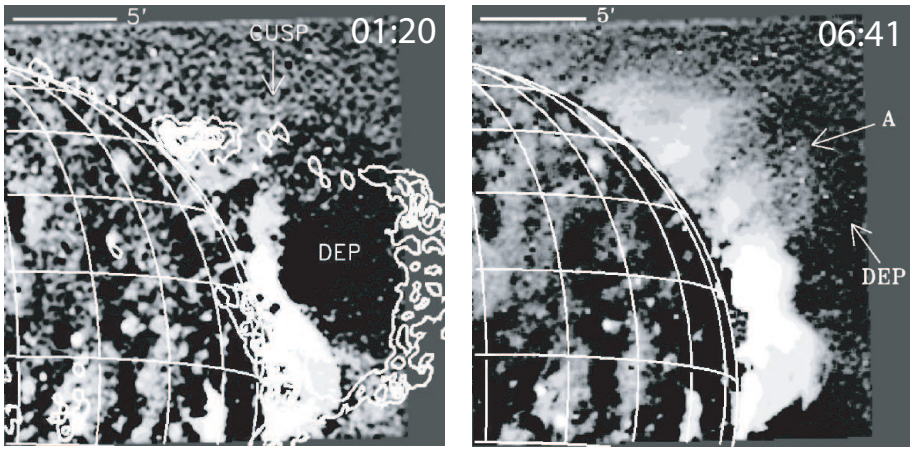

Fig. 4. The 1994 April 4-5 NoRH eruptive prominence (contour) overlaid on a soft X-ray difference image from Yohkoh showing the coronal depletion (DEP) and post-eruption arcade (A) at the limb at 1:20 UT (left) and the arcade late (6:41 UT) in the event (right) (adapted from Gopalswamy and Hanaoka, 1998).

2.2. Case Studies in the SOHO Era

2.2.1. Radio Prominence and White-Light CME

Direct comparison between NoRH prominence eruptions and white-light CMEs became possible when SOHO data became available in 1996. One of the well-observed events by various instruments was the 1997 February 6-7 CME, which consisted of all the standard features of an eruptive event. Several fragments of a filament located on a long neutral line erupted and became the core of a CME observed by SOHO/LASCO (Gopalswamy et al. 1998b). The location of the eruption on the southwest quadrant is evident from the spectacular soft X-ray post-eruption arcade (Fig.5) with the associated dimming (Gopalswamy, 1999). Figure 6 shows the CME at 03:30 UT with its familiar three-part structure. The leading edge had already crossed the LASCO FOV, but was clearly ahead of a bright blob with an extended component parallel to the limb. Superposed on this LASCO image is a 17 GHz NoRH image taken at 1:40 UT, showing that the microwave prominence was identical to the double structure in the bright core. The bright core was observed as a filament moving westward towards the limb for many hours before appearing as a prominence above the limb. The continuation of the radio prominence into the CME as its core is clear from the height-time plot of the frontal structure and the prominence core (see Fig.6). The radio and white light prominences fit to a constant acceleration curve. The frontal structure was accelerating ($\sim$17 m s^{-2}), resulting in a speed of $\sim$730 km/s at 25 R$_\odot$. The prominence had a smaller acceleration ($\sim$4 ms^{-2}) and had attained a speed of only 390 km/s at 25 R$_\odot$. The separation between the prominence and the frontal structure remained large all the way to 1 AU, as confirmed by in situ observations in the solar wind (Gopalswamy et al., 1998b).

2.2.2. Nonradial Motion of an Eruptive Prominence

A prominence core with nonradial motion on 1997 December 14 CME was studied by Gopalswamy et al. (2000). The prominence erupted from within a soft X-ray structure (ABC in Fig.7) above the southeast limb. As the eruption proceeded, the centroid of the prominence shifted equatorward with a speed of $\sim$27 km/s. The location of the prominence was at the southern foot of a helmet streamer observed by SOHO/LASCO at 00:30 UT. As the prominence erupted, the streamer showed a bulge roughly above the prominence, but the CME was fully formed with its leading edge at a CPA of 90 deg (see the LASCO image at 07:23 UT in Fig.7). Weak activity was also noted in the northern foot point of the streamer. The initial position angle of the 17 GHz prominence was $\sim$120 deg, while the white light observations placed the core at a position angle of $\sim$90 deg. That is, there was a 30 deg offset between the PE and CME position angles. The nonradial motion of the prominence suggests that the overlying streamer must have guided the eruptive prominence. Filippov et al. (2001) were able to model the eruption using a magnetic structure shown in Fig.8. They solved the equations of motion numerically to obtain the trajectory of the current carrying filament in the corona. The nonradial motion was also inferred in a statistical study by Plunkett et al. (2001) who found a bimodal distribution for the location of eruptions observed in EUV as compared to the equatorial position angle for the associated white light CMEs. It will be shown later that this bimodal distribution is confined to the solar minimum period.

2.3. A Microwave CME

A very fast eruption was detected by NoRH on 2001 April 18, originating from an active region behind the limb (9415 located about 30 deg behind the limb: S23W120). This active region had produced many energetic CMEs during its disk passage (Gopalswamy et al., 2002). The eruption in microwaves very much resembled a white light CME, with a diffuse frontal structure and a compact core.

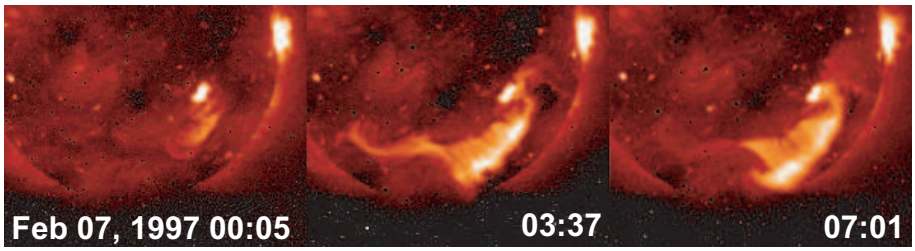

Fig. 5. Development of the post-eruption arcade during the 1997 February 07 CME as observed by Yohkoh's soft X-ray telescope.

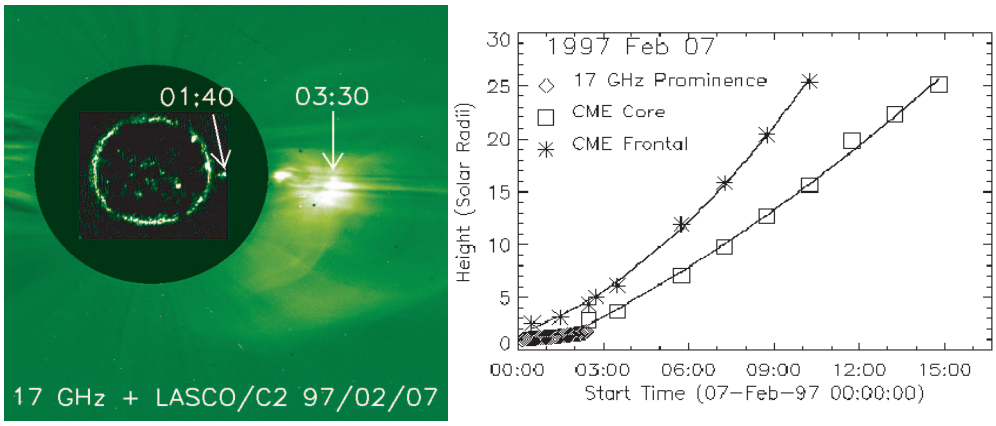

Fig. 6. *Left*: The NoRH 17 GHz eruptive prominence observed on 1997 February at 01:40 UT and its evolved form as the core of the CME observed by SOHO/LASCO/C2 at 3:30 UT. *Right*: Height-time plots of the leading edge of the CME (marked *), the NoRH prominence (diamonds) and the CME core in white light (squares).

Microwave emission appeared initially at 2:13 UT as a compact source and spread on either side of the location of initial appearance covering a position angle extent of ∼32 deg by 02:16 UT. The rapid expansion is evident in Fig.9 (left) where the loop-like appearance of the CME is the shell representing the expansion over just one minute (2:16 to 2:17 UT). When the CME first appeared in the LASCO/C2 FOV at 02:30 UT, it had an angular width of ∼70 deg at a distance of ∼5 $R_\odot$. Such early expansion is well known, and is also reflected in the mass increase up to a height of ∼8 $R_\odot$ before attaining a constant value (Vourlidas et al., 2002). The previous LASCO image at 02:06 UT had no sign of the CME. The CME had already left the C2 field of view by 02:54 UT, but appeared above the C3 occulting disk at 02:42 with the leading edge at a heliocentric distance of 7.7 $R_\odot$. Figure 9 (left) is a composite picture showing the microwave CME at 02:17 UT, becoming the white light CME at 02:30 UT (LASCO/C2) after the rapid expansion. In Fig.9 (middle), the 02:42 UT LASCO/C3 image is added, showing that the expansion has stabilized with very little increase in angular width between the C2 and C3 images. The images are 12-13 minutes apart and provide three snapshots of the rapid evolution of the CME. The microwave difference image at 02:17 UT clearly shows a core distinct from the main body of the CME. The thickness of the leading edge corresponds to the expansion in one minute. The leading edge of the microwave CME was not visible after 2:17 UT because it faded to the background level. However, the core was observed for the next 7 minutes (Fig.9 (right)). The speed of the core was ∼1635 km/s, while the average speed of the white light CME was ∼2500 km/s. It was also possible to track the core in white light. Both the core and the outer structure seem to be nonthermal microwave emission, probably due to accelerated electrons trapped in the CME magnetic structures. The core was also briefly observed in hard X-rays (Hudson et al. 2001) from lower energy electrons, while the microwave emission is from higher energy electrons.

Both the hard X-rays and microwave emission from the CME were observed because the main flare emission was occulted. Very high dynamic range would be needed to observe the diffuse CME for front side eruptions. Systematic search of such occulted fast events could provide additional information on the near surface evolution of very fast CMEs.

2.4. Evolution of a Complex CME

A filament eruption on 2001 November 17 with an unusually fast acceleration was reported by Kundu et al. (2004). NoRH was able to track the filament both on the disk and above the limb. The filament started moving outward from the southeast quadrant of the Sun around 3:30 UT with a constant acceleration (∼15 m/s^2) until about 04:45 UT, and then underwent a rapid acceleration from about 70 km/s to 425 km/s during the impulsive

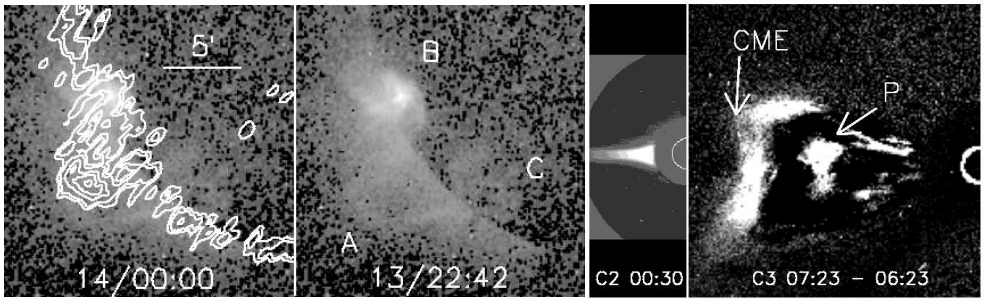

Fig. 7. The two panels on the left show the NoRH prominence (contour at 00 UT on 1997 December 14) within the soft X-ray structure (ABC at 22:42 UT on the previous day) above the southeast limb. The two panels on the right show the white light coronal streamer at 00:30 UT (December 14) and the CME with the prominence core (P) about 7 h later (07:23 UT, with the image at 06:23 UT subtracted).

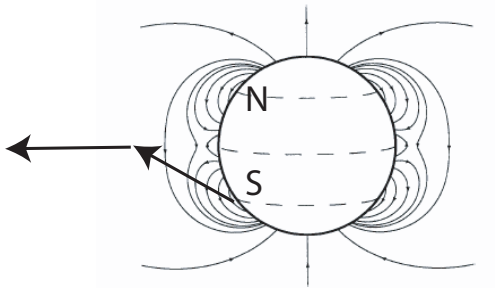

Fig. 8. The global magnetic field configuration considered by Filippov et al. (2001) to model the nonradial motion of the eruptive prominence from the location S towards the equatorial plane first and then in the equatorial plane (the trajectories shown by thick arrows). The X-ray structure ABC was located at S, while there was a dimming at N associated with the eruption. N and S were located at the northern and southern base, respectively of the streamer observed in white light.

phase of the associated flare (during 4:45 to 4:55 UT). Although the GOES X-ray flare onset was given as 4:49 UT, there was a slow rise around the time of the filament motion (see Fig.1 of Subramanian et al., 2003). The slow soft X-ray increase seems to be associated with a brightening below the filament, different from the post eruption loops in the associated active region. Kundu et al. (2004) also reported soft X-ray features moving in the direction of the filament and an X-ray dimming near the filament region around 4:31 UT. The CME first appeared in the SOHO/LASCO FOV at 3.8 $R_\odot$ at 5:30 UT and had a speed of ∼1380 km/s in the sky plane. Linear extrapolation of the height-time plot (see Fig.10) gives an onset time of 4:49 UT or slightly earlier when the projection effects are taken into account. Extrapolation of the constant speed part of the prominence trajectory yields an onset time just before 4:45 UT, coinciding with the white-light CME onset. Kundu et al. (2004) suggested that the rapid acceleration of the filament (and the associated CME) due to the flare process in the active region, similar to the scenario proposed by Zhang et al. (2001). Another possibility is that the filament might have undergone rapid acceleration due to the impact of the fast CME observed by LASCO (see Gopalswamy et al., 2001 for an example of a prominence core deflected by a fast CME). The onset of the filament eruption well before 04:00 UT and the soft X-ray loop motion followed by the dimming around 4:30 UT suggest a possible slow CME well before the observed fast CME. This would imply that the fast CME had overtaken the slow one within the occulting disk, so only a single CME was observed in LASCO field of view. Several examples of CME interaction below the occulting disk have been reported by Gopalswamy et al. (2004b).

3. Small-scale Ejecta

In addition to the CMEs and PEs, NoRH also observed other eruptive signatures such as coronal radio jets and blobs. These eruptions are generally of smaller spatial scale, some of which may be associated with PEs.

3.1. Jets

The motivation to the study of jets in microwaves came from the soft X-ray jets detected by Yohkoh (Shibata et al. 1992). Case studies of 17 GHz emission from X-ray jets were first performed by Kundu et al. (1997). The radio emission originated either from the base of the X-ray jets, or from the base and the lower part of jets. In a statistical study, Kundu et al. (1999) found an almost one-to-one correspondence between the X-ray and radio manifestations of the jets. There was also good correlation between the X-ray and microwave fluxes from the jets. The observed brightness temperature and polarization of the radio emission is generally consistent with free-free emission from the jet plasma. One of the jets showed motion in microwaves, amounting to a speed of ∼55 km/s, similar to the speeds of Hα surges. Jets are also known at other wavelengths: Wang and Sheeley (1998) found EIT counterparts of all 27 narrow (angular width 3-7 deg) CMEs observed by LASCO. Yashiro et al. (2003) identified a large number of narrow CMEs (up to 22% of all CMEs during solar maximum) when the angular width was increased to 20 deg. These narrow CMEs were similar to the normal CMEs in some respects and differed in others. Studies involving limb jets in X-rays, microwaves, EUV,

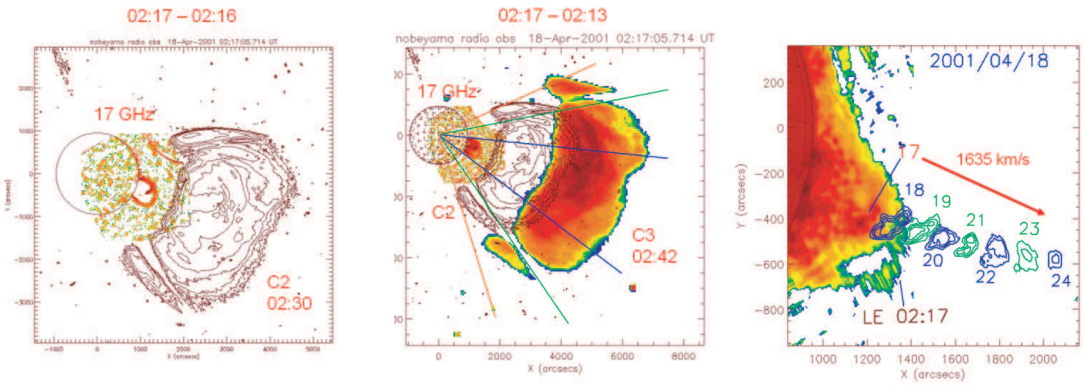

Fig. 9. *Left*: 17 GHz NoRH difference image at 2:17 UT (with the image at 2:16 UT subtracted) showing the expansion of the CME above the southwest limb. A contour image of the white light CME observed by SOHO/LASCO/C2 at 2:30 UT is superposed. The two linear features on either side of the CME are the displaced streamers. *Middle*: Same as in the left, but the NoRH image is a direct image and the LASCO/C3 image at 2:42 UT is also superposed. The position angle extent of the CME is shown by pairs of straight lines marking the edges of the CME in microwave, C2 and C3. *Right*: A small section of the corona above the southwest limb showing the microwave CME at 2:17 UT (the leading edge is marked as LE). The core at 2:17 UT is marked "17". The location of the core at subsequent times is superposed as contour images. The numbers near the contour images show the minutes after 2:00 UT. The speed (1635 km/s) and the direction of motion of the core are also indicated.

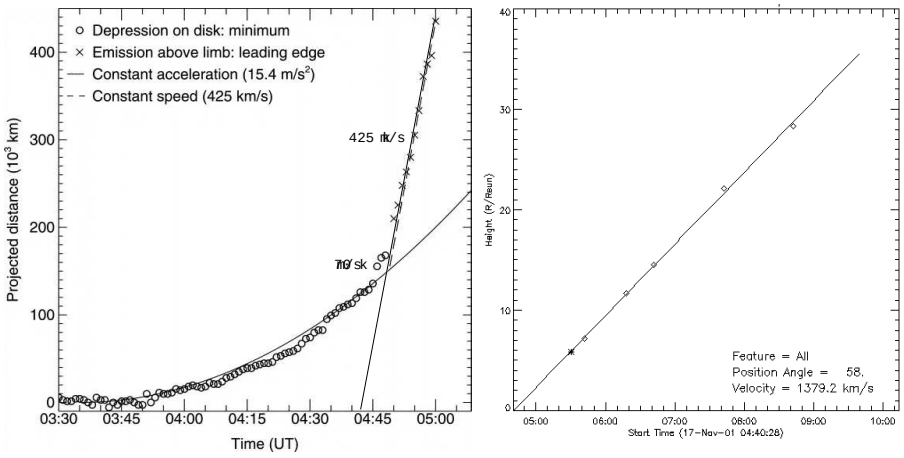

Fig. 10. *Left*: Height-time plot of the NoRH eruptive prominence on 2001 November 17 as it moved from the disk to above the limb (from Kundu et al., 2004). There was a sudden increase in speed around 4:45 UT. *Right*: Height-time plot of the LASCO CME.

and white light are needed to understand the connection between narrow CMEs and jets. The microwave data provide additional information to study the small-scale energy release, which may be similar to large eruptions, but observed with a lot of clarity.

3.2. Blobs

The appearance of compact microwave sources above a flaring loop was first reported by Shibasaki (1996) for the 1993 January 2 event. The blob was much smaller than the post flare loop in size and brightness. The blob appeared to grow out of a mound. Hori (2000) studied a few more blobs with sizes ranging from 90 to 320 arcsec. The brightness temperature was typically ∼20,000 K. Some blobs were flare remnants, while others were formed by chromospheric evaporation (or new activity). Unfortunately, some of these early events did not have CME observations to understand the overall event. Two of the events studied by Hori (2000) overlapped with SOHO observations. The 1998 May 19 event was clearly a prominence eruption and was associated with a fast CME at 1:27 UT (speed ∼600 km/s and width ∼100 deg). The CME association of this eruption was missed in the study of Gopalswamy et al. (2003a). The second event was a filament activation event with no clear ejection, and was not associated with a CME. Sometimes, blobs appeared to indicate magnetic connectivity between two mounds (Hori, 2000) and magnetic reconnection in the space between the mound and the blob. Most of the flare ejecta occur under the overall envelope of the CME, so the blob studies need to be performed again with the inclusion of CMEs to place them in the context of typical eruptions.

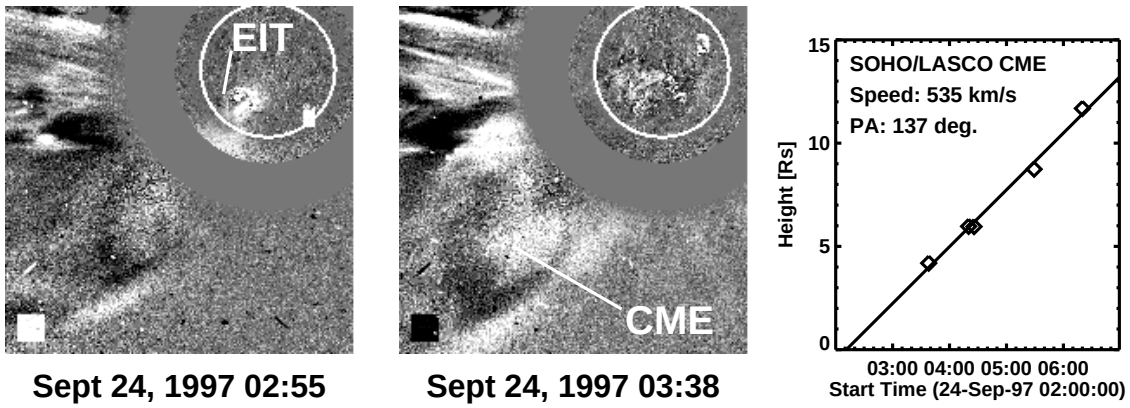

Fig. 11. The EIT brow wave of 1997 September 24 (marked EIT on the EIT difference image at 02:51 UT) with the associated white light corona from SOHO/LASCO at two times (02:55 and 03:38 UT). New material appears above the southeast limb only in the 3:38 UT LASCO frame. The height-time plot of the CME is shown on the right. The CME had an average speed of 535 km/s in the sky plane. The actual speed of the CME is likely to be much higher because of projection effects (location of the eruption at S31E19).

4. Microwave Manifestations of EIT Waves

Coronal waves in EUV, first detected by Neupert (1989), are now routinely observed by the Extreme-ultraviolet imaging telescope (EIT) on board SOHO (EIT waves - Thompson et al., 1999). The EIT waves are very helpful in identifying inner-coronal manifestations of CMEs in the spatial domain not accessible to coronagraphs. The EIT "brow waves" (so named because of their arc-like appearance in EIT images - see Gopalswamy, 2000; Gopalswamy and Thompson, 2000) are spatially and temporally coincident with metric type II radio bursts (Gopalswamy et al., 2000d). Biesecker et al. (2002) later classified the brow waves as "events with sharp brightenings" and found them to be associated with metric type II bursts, flares, and CMEs. They also found an unambiguous correlation between EIT waves and CMEs, but a significantly weaker correlation between EIT waves and flares. The brow waves are also highly likely to be associated with Moreton waves, which are chromospheric signatures. Recently, White and Thompson (2005) reported the microwave counterpart of the 1997 September 24 EIT wave using the NoRH data. They interpreted the microwave disturbance as the thermal free-free emission (optically thin) from material swept up or otherwise disturbed by the EIT wave. They also found a higher speed (835 km/s) for the microwave disturbance than for the EIT wave (500 km/s, Thompson et al., 2000).

The eruption occurred at S31E19, and the associated CME was accordingly moving in the SE direction. The sky plane speed of the CME was $\sim$ 530 km/s (see Fig.11), consistent with the EIT wave speed also measured in the sky plane. However, this speed is likely to be much smaller than the true speed due to projection effects. The true speed could exceed 1000 km/s. The CME onset has been estimated to be $\sim$02:33 UT, about 10 minutes before the onset of the EIT wave. The onset is likely to be earlier if initial acceleration and projection effects are taken into account. But the main point is the CME was expanding from the eruption site at least 10 minutes before the wave observed in EUV and microwave. At present there is no consensus on the driver of the EIT waves. Although EIT waves correlate better with CMEs than with flares, CMEs are either ignored or dismissed in some studies dealing with these waves (Hudson et al. 2003; Warmuth et al., 2004; White and Thompson, 2005). The assumption is that the EIT waves are flare blast waves. For example, White and Thompson (2005) argue that the radio emission from the EIT wave should increase if it is CME-driven, rather than the observed decrease. However, the CME is expanding and the CME brightness decreases even for accelerating CMEs. If an EIT wave surrounds the CME, the wave also expands and the radio brightness may not increase. The presence of the CME poses a problem for the blast wave scenario: since the CME is in progress when the flare starts beneath the CME, the blast wave has to move through the fast-moving CME material. This makes the shock formation difficult. Otherwise, one has to assume that the blast wave propagates only through coronal regions not occupied by the CME. Irrespective of the source of the EIT waves, their identification in microwaves is significant for further investigations (see also Aurass et al., 2002).

5. Statistical Studies of CME-PE Relationship

The case studies of solar eruptions reviewed above confirm the close relationship between CMEs and PEs. This relationship was already known from pre-SOHO observations of CMEs and Hα PEs (Webb et al., 1976; Munro et al, 1979; Webb and Hundhausen, 1987; St Cyr and Webb, 1991). However, doubts remained on this relationship until recently because some studies indicated only a minority of PEs from the disk and limb were associated with white light CMEs (Wang and Goode, 1998; Yang and Wang, 2002). Hori and Culhane (2002) and Gopalswamy et al.

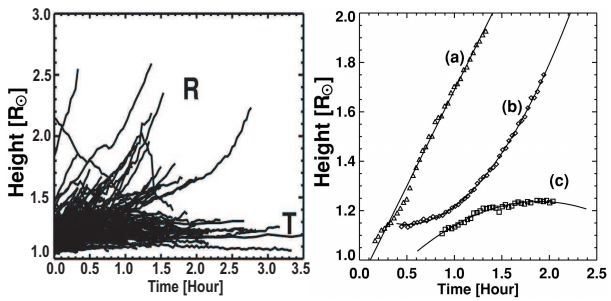

Fig. 12. *Left*: Observed trajectories of a large number of prominence eruptions (PEs). R and T represent the predominant motion in the radial and transverse directions, respectively. *Right*: The three primary types of trajectories (a) constant speed, (b) accelerating, and (c) decelerating. The heights were measured from the Sun center.

(2003a) revisited this issue using NoRH PEs. Hori and Culhane (2002) studied 50 NoRH PEs using simultaneous data available from SOHO and Yohkoh. Gopalswamy et al. (2003a) used all the 226 PEs detected automatically in NoRH images. Both confirmed the high degree of association between PEs and CMEs. These two studies used microwave PEs as the primary data set and searched for CME association, unlike most of the previous studies, which used CMEs as the primary data set. In addition to the PE-CME association, some global properties of PEs and CMEs were also investigated: latitude distribution of PEs and CMEs, position angle and onset correspondence, relation between CME cores and PEs, and solar cycle variation of PE and CME latitudes.

5.1. CME-PE Association Rate

Out of the 226 PEs were detected automatically from NoRH images between 1996 January and 2001 December, 186 overlapped with SOHO observations. The four years of NoRH data in the pre-SOHO era (before 1996) were not used due to lack of CME data. The leading edges of the PEs were tracked to the edge of the NoRH FOV (around 2.5 $R_\odot$ from the Sun center). The height-time trajectories of the PEs fell into two groups: radial (R) and transverse (T), as indicated in Fig.12. For the T events, the height remained roughly the same in time, but the prominence clearly moved horizontally from the initial location to a nearby location on the limb. It was possible to fit the trajectories either to first order or to second order polynomials (see curves marked (a), (b), (c) in Fig.12. The T events had trajectories of type (c). Linear fits were also made to all trajectories to get an average speed for statistical comparisons. The R and T events correspond to the classical "eruptive" and "active prominences", respectively (see e.g., Tandberg-Hanssen, 1995). There were 152 (or 82%) R events, while the remaining 34 (18%) were T events. The R events typically attained larger final heights or left the NoRH FOV, while the T events were confined to lower heights and never left the NoRH FOV.

Out of the 186 PEs, 144 (or 72%) were associated with SOHO/LASCO CMEs. If we consider the R events alone, the association rate increased to 83%. Clearly 52 (or 28%) events lacked white light CMEs. The CME-PE association rate is slightly lower than that (92%) obtained by Hori and Culhane (2002), but these authors used a smaller sample selected with a more restrictive criterion. The statistical results clearly confirm the close relationship originally found by Munro et al. (1979). A detailed investigation of the 52 PE events without CMEs revealed that 11 of them had changes taking place in the overlying coronal streamer (Gopalswamy et al. 2004a). The majority (7/11 or 64%) of the streamer-change PEs belonged to T events; in the R events, the PEs showed sudden stalling after traversing a small distance. The average speed and final height of the streamer-change PEs were 13 km/s and 1.19 $R_\odot$, respectively. These were intermediate between the R (65 km/s, 1.4 $R_\odot$) and T (10 km/s, 1.16 $R_\odot$) events.

5.2. PEs With and Without CMEs

The primary differences between PEs with and without associated CMEs are shown in Fig.13. On the average, PEs without CMEs attained a height of ∼1.2 $R_\odot$ compared to 1.4 $R_\odot$ for those associated with CMEs. Munro et al. (1979) had found 1.2 $R_\odot$ as the threshold height: virtually all prominences reaching this height had CME association. The CMEless PEs were also much slower (average speed ∼20 km/s) compared to the CME-associated PEs (average speed ∼70 km/s). There was also a good correlation between the final height attained and speed of PEs (correlation coefficient 0.62, see Gopalswamy et al., 2003a).

5.3. Spatial Comparison of PEs and CMEs

The NoRH images provide the exact locations of PEs, making it easy for spatial comparison between PEs and CMEs. Since the central position angle (CPA) is one of the basic attributes of CMEs, the heliographic coordinates of PEs were converted to CPAs. The CPAs of PEs and CMEs also give their respective latitudes. Since the projection effects are minimal for the limb events considered here, the latitudes derived from CPAs are expected to be accurate. Figure 14 shows that the latitude distributions of PEs and CMEs do not agree well. The latitude distribution of PEs is bimodal, whereas that of the CMEs is single peaked. This means a lack of position angle correspondence between PEs and CMEs. In order to investigate this further, the offset between the PE and CME latitudes was computed and is shown in Fig.14. The distribution of the offsets is clearly biased towards positive values suggesting that the PEs were typically located poleward of the CMEs (positive offset means the PE latitude is larger than the CME latitude). However, this offset did not occur always: it was mainly concentrated during solar minimum years, when the polar field strength is high and the global dipole of the sun is strong. It has been suggested that the strong dipolar field guides the inner coronal eruptions so that the CME observed in the coronagraphic FOV has its leading edge at lower latitude than the solar source latitude. In other words, the CMEs do not move radially away from the solar source region, as

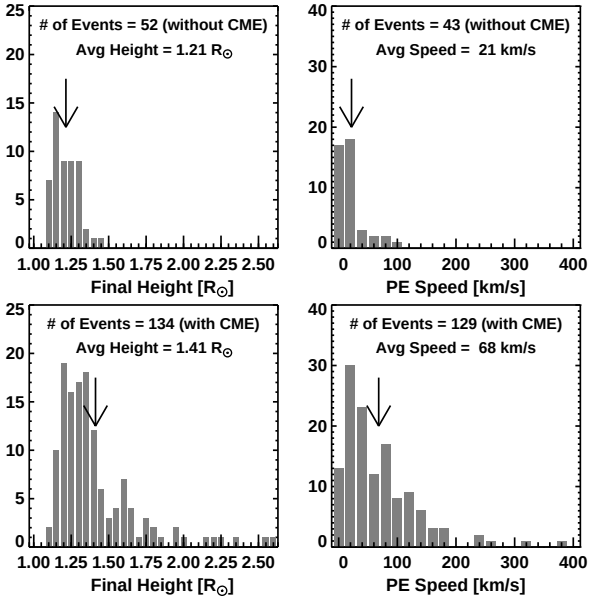

Fig. 13. Comparison of final heights (*left*) and speeds (*right*) of eruptive prominences without CMEs (top panels) with those with CMEs in the bottom panels. The average values of the distributions are marked. The final heights of prominences without CMEs never exceeded ∼0.5 $R_\odot$ from the surface, while those with CMEs reached larger heights. The CME-associated PEs were much faster than the PEs without CMEs. The speed could not be measured for all the PEs.

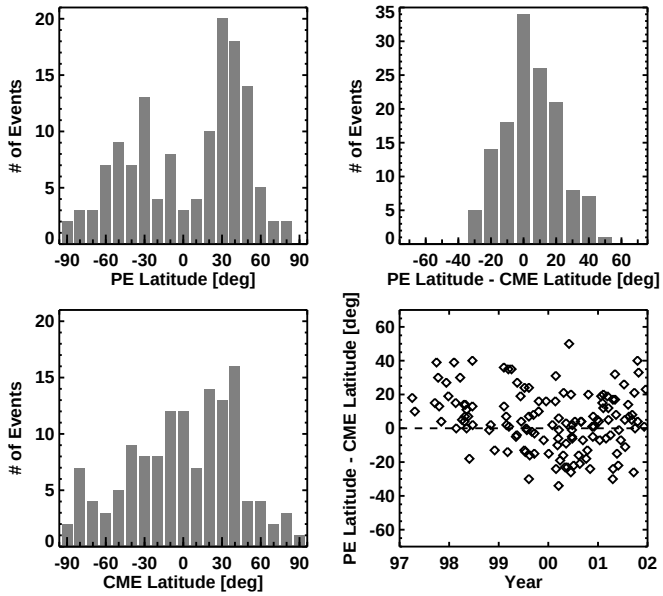

Fig. 14. *Left*: The latitude distribution of prominence eruptions compared with those of CMEs. *Right*: the offset between the central position angles of PEs and CMEs. Positive values indicate that the PEs were more poleward than were the CMEs. The offset was distinctly positive during the solar minimum phase compared to other times.

was demonstrated in a case study in section 2.2.2.

5.4. PEs and CME Core

Case studies presented here and elsewhere (Gopalswamy et al. 1998b; Hori, 2000; Srivastava et al., 2000) have clearly shown that eruptive prominences observed in the NoRH FOV become the core of the white light CMEs eventually observed at larger heights. Out of the 134 PE-associated CMEs, 98 (or 73%) had clear white-light cores (Gopalswamy et al., 2003a). This rate is slightly higher than the 65% reported by Hori and Culhane (2002) for a smaller sample. The white-light core speeds were always greater than those of the corresponding PE speeds. This is expected because of the continued acceleration (PEs generally have positive acceleration in the NoRH FOV). The average speed of PEs (∼81 km/s), white-light cores (348 km/s) and CME leading edges (609 km/s) had a definite order for all the events (Gopalswamy et al., 2003a). An exception to this was reported by Srivastava et al. (2000), in which the CME and prominence core had roughly the same speed. A scatter plot between NoRH PE speed and the speed of the corresponding white light cores showed a weak correlation: the faster the PEs the faster were their white light counterparts. As was pointed out by Hori (2000), a PE becomes a core when it remains dense enough during the transit from NoRH to LASCO FOV. PEs in streamer-change events and PEs with transverse trajectory are less likely to have cores in the LASCO FOV.

5.5. CMEs and Solar Polarity Reversal

During solar minima, most of the closed field regions (from which CMEs originate) are confined to the equatorial streamer belt. As the solar cycle progresses, closed field regions spread to all latitudes. This trend continues all the way to the solar maximum years. This pattern is clearly seen in the latitude distribution of PEs and the associated CMEs shown in Fig.15 (right). The spreading of PEs to higher latitudes is due to the "rush to the poles" of polar crown filaments (PCFs) starting in the rise phase of the solar cycle and ending somewhere during the maximum phase (see e.g. Cliver et al., 1994). The occurrence of PEs abruptly ended at high northern latitudes in October 2000 (indicated by the short vertical line between 60 and 90 deg latitudes in Fig.15 (right)). After this time, the PEs were located generally below 60 deg. In the southern hemisphere, the high-latitude PEs suddenly ended in May 2002 (indicated by the short vertical line). Clearly, there was an asymmetry in the number of PEs in the northern and southern hemispheres. The cessation of PEs at high latitudes coincided with the time of polarity reversal (Gopalswamy et al., 2003b). When all the CMEs (not just the PE-related) are grouped into high-latitude (HL, ≥60 deg) and low-latitude (LL, ≥40 deg) CMEs, the rates of HL and LL CMEs show different solar cycle variations (see Fig.15, top-left). The rate of HL CMEs is clearly related to the migration of PCFs to the poles, and the sharp decline in HL rate coincided with the polarity

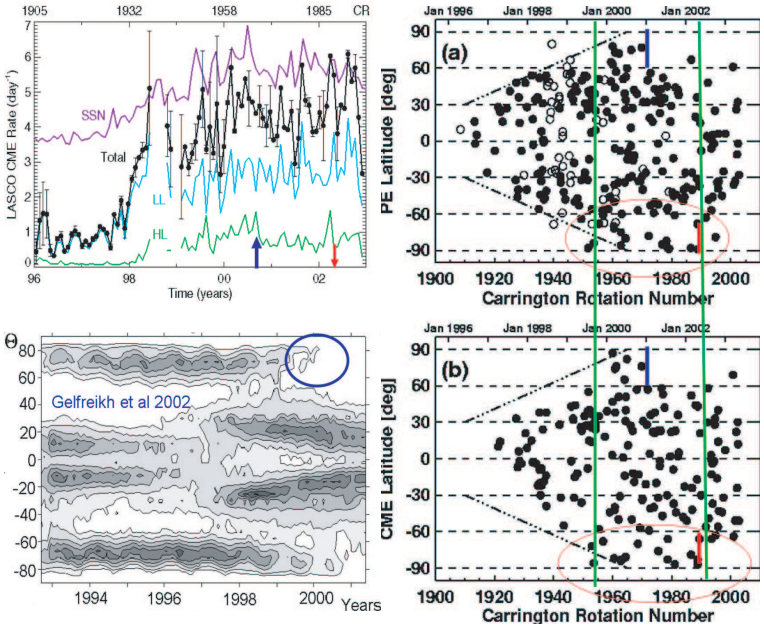

Fig. 15. Solar cycle variation of several quantities associated with solar eruptions: (top-left) The CME rates (total, high-latitude - HL, and low-latitude - LL) compared with the Sunspot number (SSN). The times of solar polarity reversal in the north (up arrow) and in the south (down arrow) Polar Regions of the Sun are shown. (bottom-left) Variation of microwave brightness as a function of time and latitude (θ) from Gelfreikh et al. 2002). The time when the northern hemispheric polar brightening disappeared is shown circled. (top-right) The latitudes of prominence eruptions (PE) and those of the associated CMEs (bottom-right) are compared. Both indicate high latitude activity up to the polarity reversal, and the sudden cessation at the time of the reversal. The short vertical lines mark the cessation of high-latitude activity. The duration of high-latitude activity is longer in the southern hemisphere (shown circled).

reversal in each pole. This close relationship between the cessation of high-latitude activity and the polarity reversal at the solar poles in cycle 23 was also found to hold for solar cycle 21 (Gopalswamy et al., 2003b). A precursor activity to the polarity reversal is the disappearance of the polar coronal holes (Harvey and Recely, 2002). In NoRH data, this precursor is seen as the cessation of polar brightenings (see the region circled in the bottom-left part of Fig.15). The microwave brightness enhancement in coronal holes is a distinct signature and may be indicative of conditions in the chromosphere favorable for solar wind acceleration (Shibasaki, 1999; Gopalswamy et al., 1999). The southern reversal occurred in 2002, beyond the data period considered by Gelfreikh et al. (2002). Thus, the high-latitude PEs and the associated CMEs provide a natural explanation for the disappearance of PCFs, which need to be removed before the poles can acquire open field structure of the opposite polarity. It must be pointed out that all the HL CMEs are PE-related, while the LL CMEs are mostly sunspot related. The LL CMEs follow the latitudinal variation of Sunspot number (SSN) because most of these CMEs originate in active regions, which contain the sunspots (confined to latitudes <45 deg). One can see that the LL CME rate is generally flat during solar maximum in contrast to the HL CME rate, which shows a sudden cessation at the time of polarity reversal in each pole. No sunspots are associated with the PCFs, so the PCF-related CMEs (or HL CMEs) are not expected to be correlated with sunspot activity.

5.6. High Latitude Eruptions and Modulation of Galactic Cosmic Rays

The increased high-latitude activity prior to the polarity reversal at solar poles has additional implications for the modulation of galactic cosmic rays (GCRs). Newkirk et al. (1981) identified CMEs as the solar origin of the low-frequency power in the interplanetary magnetic field fluctuations and suggested that the solar-cycle dependent modulation of GCRs can be explained by the presence of CME-related magnetic inhomogeneities in the heliosphere. However, the rate of CMEs known at that time (maximum rate ∼3 per day) and the minimum-to-maximum variability (by a factor of ∼6) were inadequate to cause significant GCR modulation (see the review by Wagner, 1984). Recent studies indicate that the maximum rate is as high as 6 per day and the minimum to maximum variability (by a factor of ∼10) is much higher (Gopalswamy, 2004; Lara et al., 2005). Furthermore, Newkirk et al. (1981) considered only LL CMEs (latitudes below 60 deg). As Fig.15 shows, the HL CME rate becomes almost comparable to the LL rate during solar maximum. When we consider the NoRH PEs alone, this is quite evident: The LL and HL PE rate is roughly the same during solar maximum, while the LL rate dominates during solar minimum (see Fig.16, where the NoRH PE rate is plotted since 1992). The HL CME rate may play an important role in modulating GCRs during the A>0 epochs (when the north-polar magnetic field of the Sun is

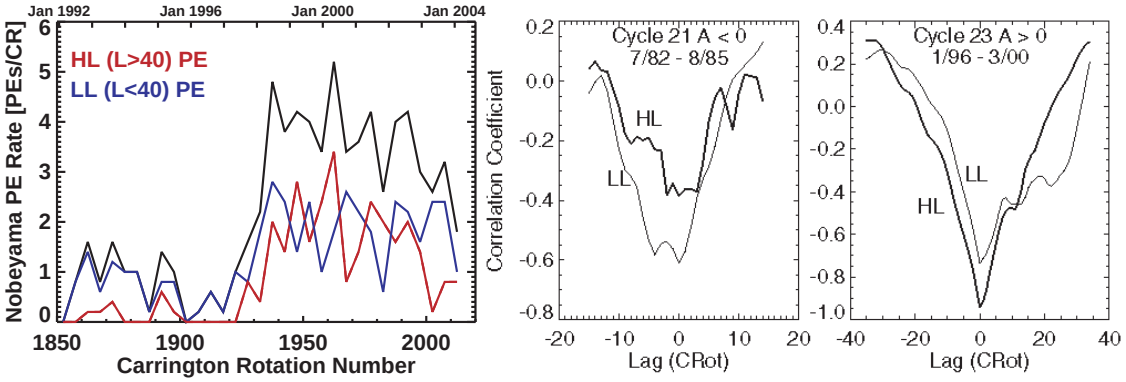

Fig. 16. *Left*: The rate of prominence eruptions (PEs) per Carrington rotation detected by NoRH. Note that the duty cycle of NoRH is only ∼8 h per day, so the actual number is expected to be much larger. The HL PEs have latitude L ≥40 deg while the LL PEs have L < 40 deg. This definition of HL PEs is slightly different from that in Fig.15. Note that the LL and HL PEs are roughly equal in number during solar maximum years compared to the solar minimum years. *right* The correlation coefficient between the CME rates (LL and HL) for the A<0 epoch cycle 21 and A>0 epoch of cycle 23. Note that the LL (HL) CME rate has a better correlation with GCR intensity in the A<0 (A>0) epoch.

northward) because the cosmic rays enter the heliosphere in the polar direction (Jokipii et al., 1977) thereby directly encountering the HL CMEs. On the other hand, the HL CMEs may not pay a role during the A < 0 epoch (when the north-polar magnetic field of the Sun is southward) because the cosmic rays enter the heliosphere along the equatorial current sheet (and hence mainly encountered by LL CMEs). The HL CME rate was found to be better (anti)correlated with the GCR intensity than the LL CMEs for the SOHO CMEs during the A>0 epoch of cycle 23 (see Fig.16). When the available CME data for the A <0 epoch in cycle 21 were examined, the relative importance was reversed: the LL CMEs were better (anti)correlated with the GCR intensity. While this work is preliminary, it certainly suggests the possibility of obtaining a better physical picture of the GCR modulation process. The continued operation of NoRH through the A ¡0 epoch will provide uniform PE data to confirm this important result. The role of CMEs is also bolstered by the recent result that global merged interaction regions (GMIRs) did not form (Richardson et al., 2005) during the intense eruptive activity during October November 2003 (Gopalswamy et al., 2005). When GMIRs do not form, the HL CMEs represent a major alternative for GCR modulation in the polar region.

6. Concluding Remarks

The NoRH observations have provided several key inputs to the ongoing study of CME initiation by observing one of the essential substructures of CMEs, viz., the prominence core. This is especially important because NoRH can observe both the per-eruptive and eruptive phases of prominences. Additional information simultaneously available on the post-eruption arcades has proved to be extremely useful in deriving physical conditions prevailing at the eruption site. The uniform and uninterrupted observation of NoRH for ∼8 h per day has enabled better comparison with data at other wavelengths (such as X-rays and EUV) obtained in overlapping fields of view. Although the spatial resolution of microwave images is not as high as that in Hα images, they can provide much better information on eruptive prominences because of the continuum nature of the radiation. Estimating the prominence mass from radio observations is a useful tool, which when compared with the CME core can provide early information on CMEs. A quantitative comparison between PEs and the associated white-light cores should help understand the fraction of prominence mass escaping the Sun and how it compares with the overlying frontal structure observed in white light. Although the microwave PEs and the white-light cores had little spatial overlap at present, future instruments such as the COR1 telescope on board the STEREO mission are expected to have a reasonable overlap with NoRH FOV. Thus, continued operation of NoRH during the STEREO mission will greatly enhance CME studies. For example, one should be able to observe the nonradial motion of CMEs overlying the nonradial PEs commonly observed by NoRH. Another important quantity will be the starting heights of CMEs. Combination of NoRH and Yohkoh data has shown that CMEs start typically from a height of ∼0.3 $R_\odot$ from the surface. This can be verified when CME observations become available from COR1, whose inner edge of the field of view is close to this (0.4 $R_\odot$ from the solar surface).

Continued operation of NoRH is also important for joint studies with the Solar-B data. One of the weaknesses of CME studies is the magnetic properties of CMEs at and before the eruption. Since Solar-B will provide such information, combining it with filament data from NoRH should be able to fill this gap. While the limb data from NoRH have been well utilized for CME studies, the disk data have not been fully exploited. With the aid of sophisticated imaging techniques, it may be possible to identify filament signatures indicative of potential eruptions. Such information will also be useful for space weather purposes because disk CMEs are the ones that impact Earth.

Quantitative information on the high-latitude PE rate became available for the first time during the A>0 epoch during cycle 23, which led to the discovery of the coincidence between solar polarity reversal and the cessation of high-latitude activity. In order to confirm this result, NoRH PE data are needed at least through the next solar maximum (around the year 2012), when the Sun will reverse its polarity and enter into the A>0 epoch. In addition, this will also provide an opportunity to verify the tandem influence of high and low-latitude activities on cosmic rays presented with noisy data in Fig.16.

The author would like to thank his long term collaborators Y. Hanaoka, M. Shimojo and K. Shibasaki. He is also grateful to the hospitality extended by S. Enome, T. Kosugi, and K. Shibasaki during his visits to the Nobeyama Radio Observatory. The author also thanks S. Yashiro and S. Akiyama for help in preparing some of the figures, and A. Asai for formatting the text.

References

Anzer, U., and Pneuman, G.W., Solar Phys. 79, 129, 1982

Aurass, H., Shibasaki, K., Reiner, M., & Karlicky, M., ApJ, 567, 610, 2002

Biesecker, D. A., Myers, D. C., Thompson, B. J., Hammer, D. A., ApJ, 569, 1009, 2002

Cliver, E. W., St. Cyr, O. C., Howard, R. A., and McIntosh, P. S., in Solar coronal structures, ed. V. Rusin, P. Heinzel & J.-C. Vial, VEDA Publishing House of the Slovak Academy of Sciences, p.83, 1994

Cliver, E. W. and Hudson, H. S., . Atmospheric Terrest. Phys., 64, 231, 2002

Cremades, H. and Bothmer, V., Astron. Astrophys., 422, 307, 2004

Filippov, B. P., Gopalswamy, N. and Lozhechkin, A. V., Solar Phys., 203, 119, 2001

Gelfreik, G., Makarov, V., Tlatov, A. G., Riehokainen, A., Shibasaki, K., Astron. Astrophys. 389, 618, 2002.

Gopalswamy, N., in 'Solar Physics with Radio Observations', ed. T. Bastian, N. Gopalswamy and K. Shibasaki, p. 141, 1999.

Gopalswamy, N., in Radio Astronomy at Long Wavelengths, Geophysical Monograph 119, AGU, Washington DC, p.123, 2000.

Gopalswamy, N., Adv. Space Res., 31 (4), 869, 2003

Gopalswamy, N. in "The Sun and the Heliosphere as an Integrated system", ASSL series, edited by G. Poletto and S. Suess, KLUWER/Boston, Chapter 8, p. 201, 2004

Gopalswamy, N. and Thompson, B. J., J. Atmospheric Terrest. Phys., 62, 1457, 2000.

Gopalswamy, N., Kundu, M. R., Hanaoka, Y., Enome, S., Lemen, J. R., and Akioka, M. New Astron., 1, 207, 1996

Gopalswamy, N., Hanaoka, Y., Kundu, M. R., Enome, S., Lemen, J. R., Akioka, M. and Lara, A., ApJ, 475, 348, 1997

Gopalswamy, N. and Hanaoka, Y., ApJ, 498, L179, 1998

Gopalswamy, N., Hanaoka, Y. and Lemen, J. R., in New Perspectives on Solar Prominences, edited by D. F. Webb, B. Schmieder, and D. M. Rust, p. 358, 1998a

Gopalswamy, N., et al., Geophys. Res. Lett., 25, 2485, 1998b

Gopalswamy, N.; Shibasaki, K.; Thompson, B. J.; Gurman, J.; DeForest, C., J. Geophys. Res., 104, 9767, 1999

Gopalswamy, N., Hanaoka, Y., and Hudson, H. S., Adv. Space Res. 25, 1851, 2000a

Gopalswamy, N., Kaiser, M. L., Sato, J., and Pick, M., in High Energy Solar Physics, Ed. R. Ramaty and N. Mandzhavidze, PASP Conf Ser., vol. 206, p. 355, 2000b.

Gopalswamy, N., Yashiro, S., Kaiser, M. L., Howard, Bougeret, J.-L., ApJ, 548, L91, 2001

Gopalswamy, N., Yashiro, S., Michalek, G., Kaiser, M. L., Howard, R. A., Reames,D. V., Leske, R. and Von Rosenvinge, T., ApJ, 572, L103, 2002.

Gopalswamy, N., Shimojo, M., Lu, W., Yashiro, S., Shibasaki, K., Howard, R. A., ApJ, 586, 562, 2003a

Gopalswamy, N., Lara, A., Yashiro, S., Howard, R. A., ApJ, 598, L63, 2003b

Gopalswamy, N., Shimojo, M., Lu, W., Yashiro, S., Shibasaki, K., Howard, R. A., Adv. Space Res., 33(5), 676, 2004a

Gopalswamy, N., Yashiro, S., Krucker, S., Stenborg, G.; Howard, R. A., J. Geophys. Res., 109, A12, CiteID A12105, 2004b

Gopalswamy, N., Yashiro, S., Liu, Y., Michalek, G., Vourlidas, A., Kaiser, M. L., and Howard, R. A., J. Geophys. Res., 110, A09S15, 2005

Hanaoka, Y. et al. PASJ, 46, 205, 1994

Hanaoka, Y. and Shinkawa, T., ApJ,510, 466, 1999.

Harvey, K., and Recely, F., Solar Phys., 211, 31, 2002

Hori, K, Adv. Space Res., 26(3), p. 481, 2000.

Hori, K., and Culhane, J. L., A&A, 382, 666, 2002

Hudson, H. S., Kosugi, T., Nitta, N., and Shimojo, M., ApJ, 561, L211, 2001

Hudson, H. S., Khan, J. I., Lemen, J. R., Nitta, N. V., & Uchida, Y., Solar Phys., 212, 121, 2003

Jokipii, J. R., Levy, E. H., and Hubbard, W. B., Astrophys. J., 213, 861, 1977

Kundu, M. R., Shibasaki, K., and Nitta, N., ApJ, 491, L121, 1997

Kundu, M. R. et al., ApJ, 520, 391, 1999

Kundu, M. R., White, S. M., Garaimov, V. I., Manoharan, P. K., Subramanian, P., Ananthakrishnan, S., Janardhan, P. ApJ, 607, 530, 2004.

Lara, A., Gopalswamy, N.,. Caballero-Lopez, R., Yashiro, S., and Valdes-Galicia, J., ApJ, 625, 441, 2005.

Munro, R. H., Gosling, J. T., Hildner, E., MacQueen, R. M., Poland, A. I., and Ross, C. L., Solar Phys., 61, 201, 1979

Nakajima, H. et al., Proc. EEE, 82, 705, 1994

Neupert, W. M., ApJ, 344, 504, 1989

Newkirk, G., Hundhausen, A. J. and Pizzo, V., J. Geophys. Res., 86, 5387, 1981

Plunkett, S. P., Thompson, B. J., St. Cyr, O. C., and Howard, R. A., J. Atmospheric Terrest. Phys., 63, 389, 2001.

Richardson, J. D., Wang, C. Kasper, J. C., and Liu, Y. Geophys. Res. Lett., 32, L03S03, 2005.

Shibasaki, K., in Magnetic reconnection in the Solar Atmosphere, ed, R.D. Bentley and J. Mariska, ASP conf., p. 176, 1996

Shibasaki, K., in Proceedings of the Nobeyama Symposium, held in Kiyosato, Japan, Oct. 27-30, 1998, Eds.: T. S. Bastian, Gopalswamy, N. and Shibasaki, K., NRO Report No. 479., p.1-9, 1999

Shibata, K., et al., PASJ, 44, L173, 1992

Srivastava, N., Schwenn, R., Inhester, B., Martin, S. F., and Y. Hanaoka, ApJ, 534, 468, 2000.

St. Cyr, O. C. and Webb, D. F., Solar Phys., 136, 379, 1991
Svestka, Z. and Cliver, E. W., in Proc. IAU Colloquium 133, edited by Z. Svestka, B. V. Jackson and M. Machado, M., Springer-Verlag, Berlin, p. 1, 1992.
Subramanian, P., Ananthakrishnan, S., Janardhan, P., Kundu, M. R., White, S. M., and Garaimov, V. I., Solar Phys., 218, 247, 2003.
Tandberg-Hanssen, E., The nature of solar prominences, Kluwer, Dordrecht, 1995.
Thompson, B. J., et al., ApJ, 517, L151, 1999
Thompson, B. J., et al., Solar Phys., 193, 161, 2000.
Uralov, A.M., Lesovoi, S. V., Zandanov, V. G., and Grechnev, V. V., Solar Phys., 208, 69, 2002
Vourlidas, A., Buzasi, D., Howard, R. A., & Esfandiari, E., Solar variability: from core to outer frontiers, Ed. A. Wilson. ESA SP-506, Vol. 1. Noordwijk: ESA Publications Division, p. 91, 2002.
Wagner, W. J., Ann. Rev. Astron. Astrophys., 22, 267, 1984
Wang, H., and Goode, P. R., ASP Conf. Ser. 140: Synoptic Solar Physics, 140, 497, 1998.
Wang, Y.-M. and Sheeley Jr., N. R., ApJ, 575, 542, 1998
Warmuth, A., Vrs nak, B., Magdalenic', J., Hanslmeier, A., and Otruba, W. Astron. Astrophys. 418, 1117, 2004
Webb, D. F., Krieger, A. S., and Rust, D. M., Solar Phys., 48, 159, 1976
Webb, D. F. and Hundhausen, A. J., Solar Phys., 108, 383, 1987
White, S. M. and Thompson, B. J., ApJ, 20, L63, 2005
Yang, G. and Wang, H., Solar-Terrestrial Magnetic Activity and Space Environment, 113, 2002
Yashiro, S., Gopalswamy, N. Michalek, G., and Howard, R. A., Adv. Space Res., 32(12), 2631, 2003
Zhang, J., Kundu, M. R., White, S. M., Dere, K. P., and Newmark, J. S., ApJ, 561, 396, 2001.